Nanoscale

PAPER

View Article Online
View Journal | View Issue

Cite this: *Nanoscale*, 2019, **11**, 15120

Self-assembly of collagen bundles and enhanced piezoelectricity induced by chemical crosslinking†

Malavika Nair, Yonatan Calahorra, Sohini Kar-Narayan, Serena M. Best and Ruth E. Cameron *

Received 4th June 2019,
Accepted 15th July 2019

DOI: 10.1039/c9nr04750f

rsc.li/nanoscale

The piezoelectricity of collagen is purported to be linked to many biological processes including bone formation and wound healing. Although the piezoelectricity of tissue-derived collagen has been documented across the length scales, little work has been undertaken to characterise the local electromechanical properties of processed collagen, which is used as a base for tissue-engineering implants. In this work, three chemically distinct treatments used to form structurally and mechanically stable scaffolds—EDC-NHS, genipin and tissue transglutaminase—are investigated for their effect on collagen piezoelectricity. Crosslinking with EDC-NHS is noted to produce a distinct self-assembly of the fibres into bundles roughly 300 nm in width regardless of the collagen origin. These fibre bundles also show a localised piezoelectric response, with enhanced vertical piezoelectricity of collagen. Such topographical features are not observed with the other two chemical treatments, although the shear piezoelectric response is significantly enhanced upon crosslinking. These observations are reconciled by a proposed effect of the crosslinking mechanisms on the molecular and nanostructure of collagen. These results highlight the ability to modify the electromechanical properties of collagen using chemical crosslinking methods.

1 Introduction

As the primary structural protein in mammalian tissues, there has been significant interest in the physical properties of collagen, including its inherent piezoelectricity. It has been suggested that the piezoelectric nature of collagen plays a role in various biological processes including bone formation, resorption[1] and wound healing.[2,3] The ubiquity of collagen across various tissues also makes collagen a viable base material for tissue engineering applications. In such applications, the collagen-based device is routinely crosslinked to provide the durability and mechanical integrity needed for the intended duration of service.

Although research on collagen piezoelectricity has burgeoned over the last five decades, the hierarchical structure of collagen has posed a challenge in deciphering the origins of its piezoelectric effect.[4–6] The earliest measurements of collagen's piezoelectric coefficients by Fukada *et al.* describe the ability of collagen to naturally form highly aligned oriented fibres[5] resulting in one of the highest piezoelectric responses (12 pC N^{-1}) observed in ordered natural biopolymers.[7]

More recent work has attempted to underpin the molecular origins of collagen piezoelectricity through atomistic modelling and piezoresponse force microscopy (PFM). From molecular dynamics simulations of collagen molecules and microfibrils[8] to the measurement of piezoelectricity in isolated collagen fibrils,[7,9,10] the piezoelectricity of highly aligned collageneous tissues have been traced back to the observed fibrillar packing and bonding. Further measurement of native tissues has also led to understanding of the link between the piezoelectric behaviour and mechanical properties, particularly with the advent of piezoresponse force microscopy. For instance, when combined in hamstrings, fibrils of opposing polarity are electrostatically attracted to one another and result in a shear piezoelectric response from charge accumulation, whereas those with similar polarity repel, which can result in different mechanical behaviours by facilitating or inhibiting the slipping of fibrils.[11] This slipping behaviour has also been investigated in the 'rough' ultrastructure of biopolymers, including collagen fibrils, where the slipping corresponds to the fibril *D*-spacing and is suggested to play a role in the toughness of the materials.[12]

Advanced atomic force microscopy techniques have seen an improvement in both the ability to characterise materials at unprecedented resolutions as well as the ability to map electromechanical properties of the material onto the topographical features across the surface.[13] Of these techniques, the use of peak force (PF) tapping allows the probe to intermittently

University of Cambridge, Department of Materials Science and Metallurgy, 27 Charles Babbage Road, Cambridge, CB3 0DS, UK. E-mail: rec11@cam.ac.uk, smb51@cam.ac.uk

†Electronic supplementary information (ESI) available. See DOI: 10.1039/C9NR04750F

contact the sample to measure instantaneous forces as low at 10^{-12} N.[14] The ability to raster an oscillating tip across the surface allows a force–distance curve to be produced at each pixel as seen in Fig. 1, enabling the creation of mechanical property-maps with spatial resolution.

The low force applied in PF also enables it to be used to image biological samples such as cellulose nanowires,[15] synthetic piezoelectric polymers like PVDF[16,17] and Nylon,[18] as well as polymers for biomedical uses like poly-L-lactic acid.[19] Similarly, the piezoelectric properties of the sample can be obtained using piezoresponse force microscopy (PFM), where an alternating voltage bias is applied on the tip whilst in contact with the sample.[20] From the deflection, buckling and torsion of the cantilever in response to the surface topography and piezoelectric response, the out-of-plane (vertical) and in-plane (lateral) piezoresponse signal can be recorded.

To take into account any concurrent electrostatic effects between the surface and the AFM tip, Kelvin Force Probe Microscopy (KPFM) is also performed in lift mode, to obtain the surface potential of the samples. This value can then be offset as a DC bias against the AC signal during the PFM measurement so that the true piezoresponse can be measured without interfering electrical phenomena.[21] The true effect of a shear or normal piezoelectric response in the sample can be distinguished as seen in Fig. 1.

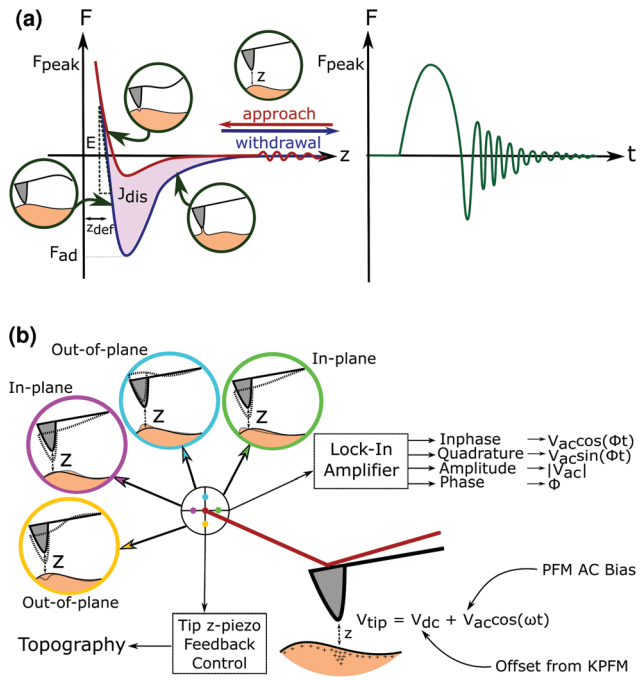

Fig. 1 Schematics of quantitative nanomechanical mapping and piezoresponse force microscopy. (a) A schematic of the QNM 'heartbeat': a peak force tapping cycle consists of an approach and withdrawal giving rise to a force (F)–distance (z) curve. This force distance curve reflects three key features: F_{max}, the peak force achieved during a tapping cycle, F_{ad} the adhesion force, J_{dis} the dissipation energy, z_{def} is the deformation, and E is the elastic modulus. (b) A schematic of the PFM measurement: an AC bias is applied to a conductive tip, inducing a polarisation in piezoelectric samples. By connecting a position sensitive detector to a lock-in amplifier, the deflection, torsion and buckling of the cantilever in and out of the plane can be converted into a lateral piezoresponse signal, decoupled from the topography maintained at a constant height by the z-piezo feedback control. A DC offset corresponding to interactions between the sample and tip can be applied after surface potential measurement from KPFM.

Processed collagen can most readily be studied in the form of cast films, which act as a 2D surrogate for more complex geometries.[22,23] Measurements on films enable us to identify the properties specific to the bonding in collagen as opposed to the distribution of larger units across 3D space. Hydrated collagen films can be characterised by a complex piezoelectric response, with mechanical effects such as the relaxation of non-piezoelectric phases, affecting the piezoelectric properties of the surrounding piezoelectric phase.[24] Aside from some research on extruded collagen fibres collagen[25] little to no prior work has considered the effect of external modifications on the piezoelectric response of collagen.

Chemical crosslinking of tissue engineering constructs results in the modification of the collagen bonding in order to produce stable structures. The mechanism of action of the active agent in the crosslinker may result in the modification of chemical groups that contribute to the overall charge distribution along the collagen peptide backbone.[6] In this study, EDC-NHS, genipin and tissue transglutaminase (TG2), three crosslinkers with distinct reaction chemistries[26–28] are investigated for their ability to alter the piezoelectricity of collagen. EDC-NHS utilises carboxylic acid and amine side groups in collagen (lysines, aspartic and glutamic acids) to form an amide bond, whereas genipin reacts with two lysines to form a crosslink. TG2 converts a glutamine to a glutamic acid, which may then undergo further reactions depending on the conditions of crosslinking.[29] However, understanding the ways in which the piezoelectricity of collagen may be affected by the crosslinking process and exploited in practice for tissue engineering applications remains in its infancy.

With the use of quantitative nanomechanical mapping, Kelvin probe force microscopy and piezoresponse force microscopy, the effect of altering amino acids on collagen substrates are characterised for the first time in engineered collagen constructs. This paper therefore represents the first experimental confirmation of the amino acid level modification of collagen piezoelectricity, as well as the ability to modify these in practice using common tissue engineering crosslinkers.

2 Results

2.1 Quantitative nanomechanical mapping

Quantitative Nanomechanical Mapping (QNM) was used to detect the sample topography and mechanical properties (modulus, dissipation, adhesion and deformation) of non-crosslinked and crosslinked insoluble collagen films in dry conditions. Representative topography channels are shown in

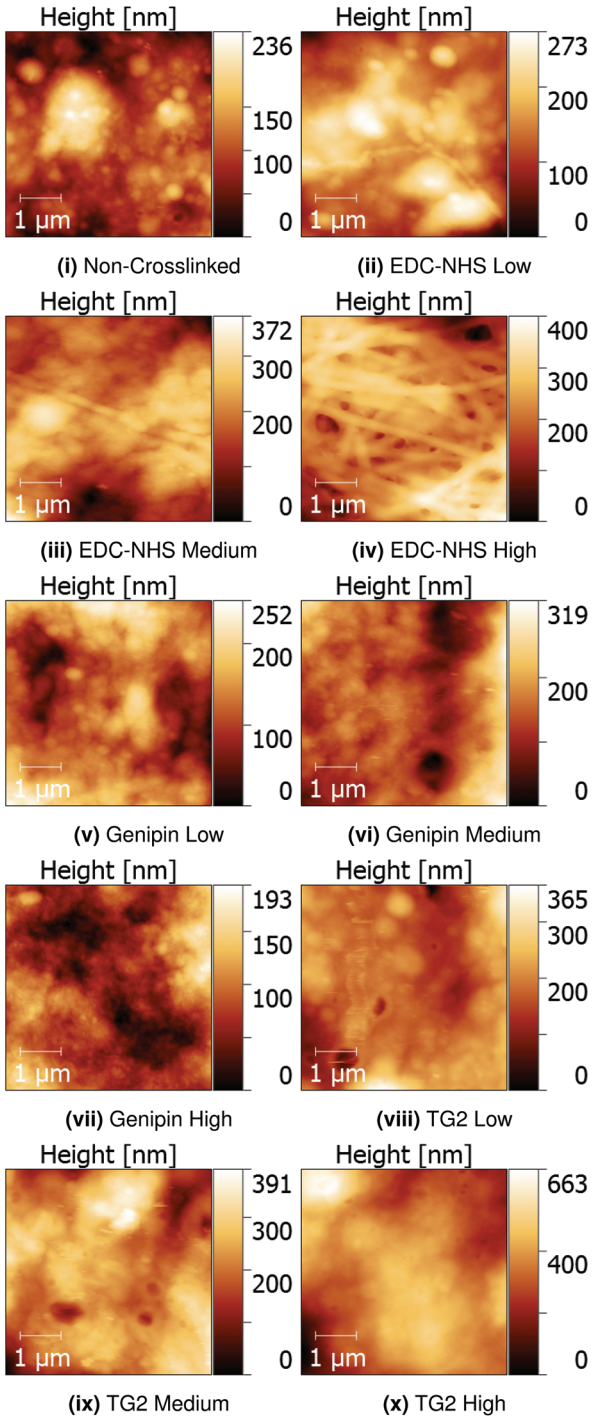

Fig. 2 QNM topography channels of non-crosslinked and EDC-NHS, genipin and transglutaminase crosslinked samples on borosilicate glass. Fibre bundles are only produced with increasing EDC-NHS crosslinking.

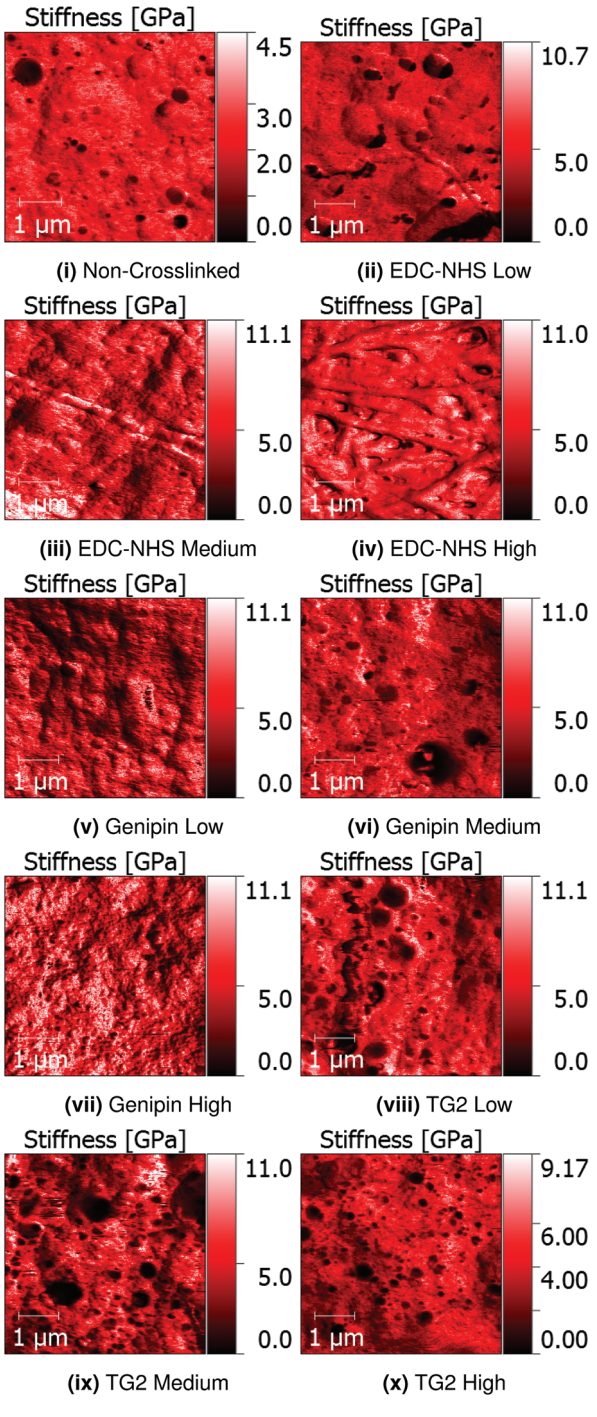

Fig. 3 QNM stiffness channels of non-crosslinked and EDC-NHS, genipin and transglutaminase crosslinked samples on borosilicate glass. Bubbles appear are dark circular areas, whereas both the fibres bundles and matrices possess a homogeneous modulus across the films.

Fig. 2. The non-crosslinked samples are noted to be rough, with no distinct featuring visible on the surface, aside from trapped air bubbles underlying the surface. Such bubbles appear as roughly circular areas of low stiffness in Fig. 3.

Samples crosslinked using EDC-NHS produced fibre bundles of roughly 300 nm in width. Such bundles only appeared in collagen films crosslinked in EDC-NHS, with a greater density of fibres, with higher crosslinking concentration as seen in Fig. 2ii–iv. Samples crosslinked using genipin or transglutaminase did not exhibit any significant changes in the roughness of the surface upon treatment when compared with the non-crosslinked films.

The averages of the median values measured for the moduli for cast films is plotted in Fig. 4. Only the values on borosilicate glass are considered here since maximum value saturation was observed with some samples on ITO coated glass.

Statistically significant differences are noted in the average of the median modulus of a film after crosslinking with all concentrations of EDC-NHS, the highest concentration of genipin as well as low concentrations of TG2. Higher concentrations of TG2 did not result in statistically significant changes to the elastic modulus. Large variations within and across samples as seen in Fig. 21† as well as the semi-quantitative nature of the technique.

2.2 Piezoresponse force microscopy

A comparison of the average signal from the vertical inphase response and surface potential are shown in Fig. 5. No significant differences were seen in the lateral inphase channels for the crosslinked materials when compared with the non-crosslinked insoluble collagen. However, a significant difference in the vertical inphase channel was observed in the TG2- and genipin-crosslinked films when compared with both the soluble collagen and insoluble collagen as controls. Averages of the lateral inphase and amplitude are shown in ESI, Fig. 20.†

Representative images comparing the topographical correlation of insoluble collagen and EDC-NHS crosslinked insoluble collagen with their piezoelectric responses are shown in Fig. 6a. Insoluble collagen exhibited distinct piezoelectric domains in both the lateral inphase and lateral amplitude

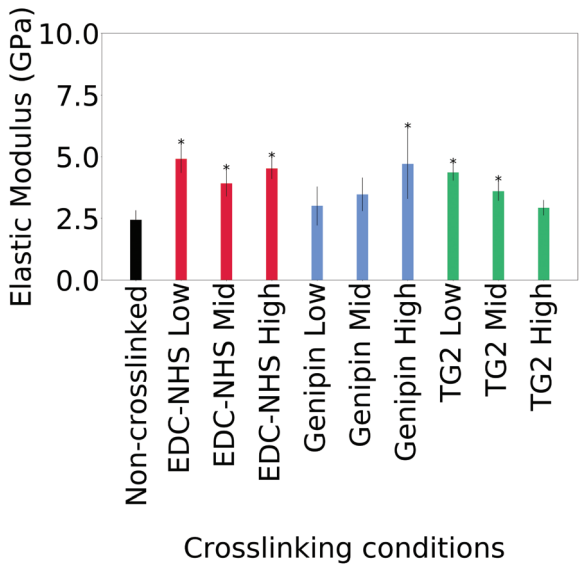

Fig. 4 Numerical average of the elastic modulus of non-crosslinked and treated insoluble collagen samples. Significant differences for all conditions of crosslinking except the low and intermediate values of genipin and high values of TG2, when compared with the non-crosslinked collagen. An asterisk (*) indicates $p < 0.05$ with respect to the non-crosslinked insoluble collagen condition.

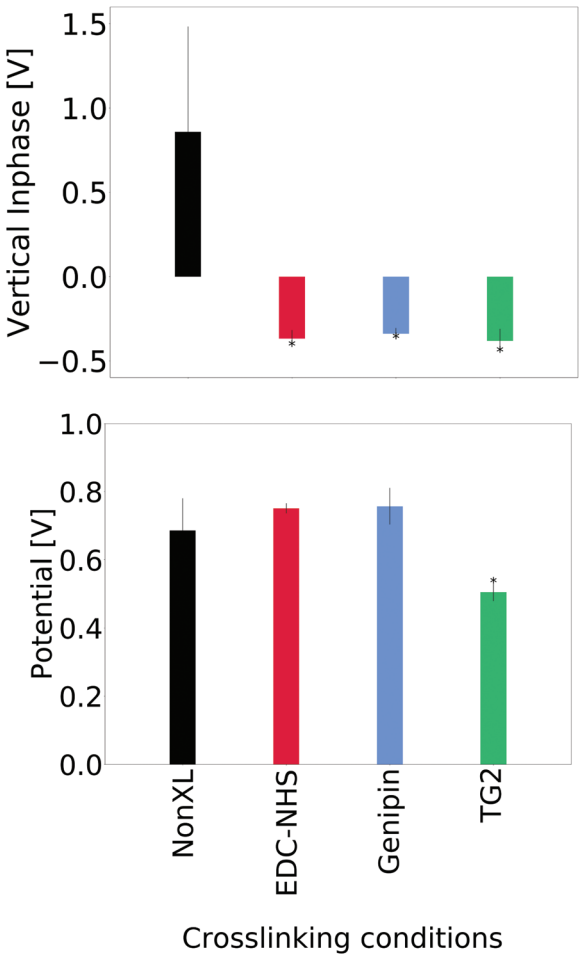

Fig. 5 Numerical averages of the piezoelectric response across non-crosslinked and treated insoluble collagen samples. Significant differences are seen in the vertical inphase channels displayed here upon crosslinking with all conditions. The surface potential on the other hand is only seen to decrease significantly for TG2-treated samples. An asterisk (*) indicates $p < 0.05$ with respect to the non-crosslinked insoluble collagen.

channels. Such domains were not observed with the vertical inphase channel of the non-crosslinked insoluble collagen. These piezoelectric domains exhibited no correlation with topographical features on the film surface.

Conversely, a distinct localised response was observed where large collagen bundles arising from EDC-NHS crosslinking were present as seen in Fig. 6b. The lateral inphase revealed little topographical correlation upon crosslinking, suggesting a localisation of the vertical piezoelectric response upon crosslinking with EDC-NHS.

The localisation was not accompanied by any systematic change in the piezoelectric response of fibre bundles across the crosslinked films, since individual fibre bundles of both increased and decreased lateral amplitude were observed. Disparate components were also measured for both transverse and parallel orientations of the fibre bundles across the vertical inphase and lateral inphase channels, further suggesting

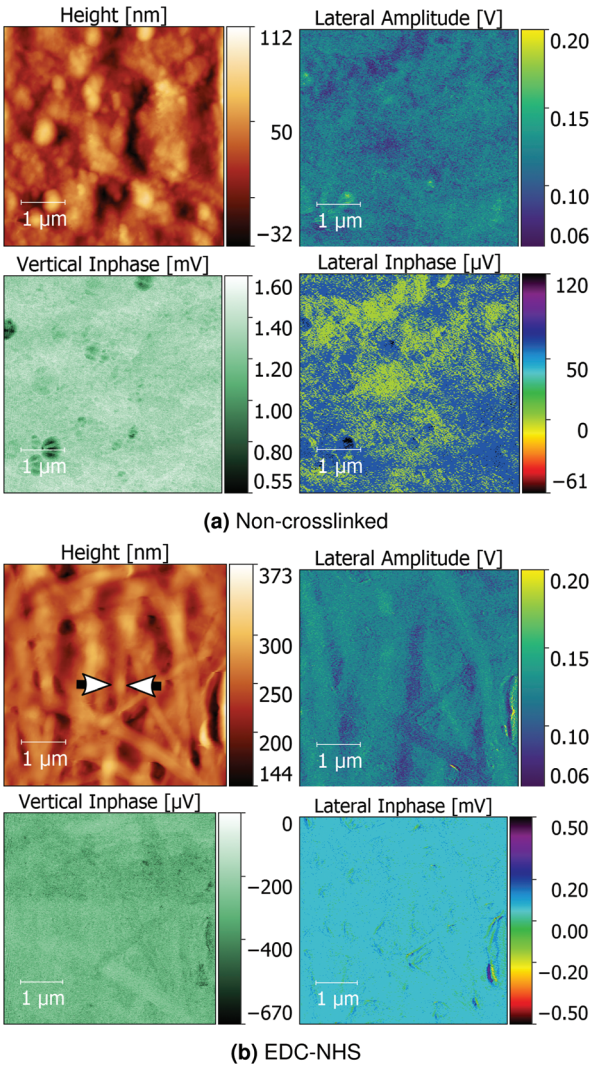

Fig. 6 Piezoelectric response from insoluble collagen fibrils when (a) non-crosslinked (b) crosslinked with EDC-NHS. Piezoelectricity is homogeneous and random in all conditions except along the EDC-NHS fibre bundles, which produce localised piezoelectricity. Arrows indicate fibre bundles of ~300 nm formed upon crosslinking.

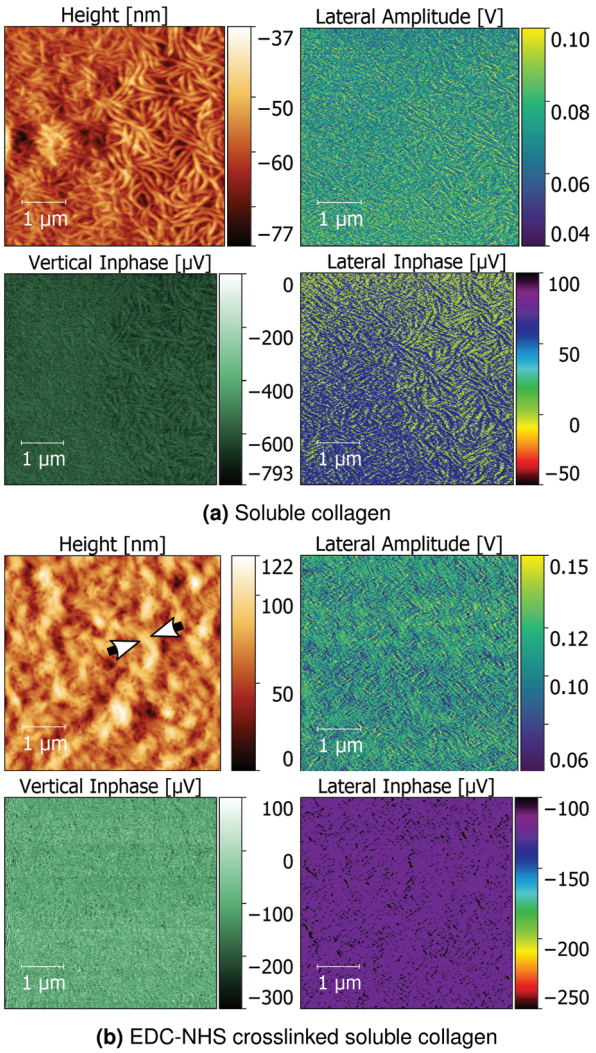

Fig. 7 Topography, lateral amplitude, vertical inphase and lateral inphase of (a) soluble collagen and (b) EDC-NHS crosslinked soluble collagen. Arrows indicate fibre bundles of ~300 nm formed upon crosslinking with EDC-NHS.

the strong correlation of the signal with the topographical features.[30]

Unlike crosslinking with EDC-NHS, TG2 and genipin did not produce any topographical correlation in the piezoelectric response (ESI, Fig. 14–19†).

Additionally, soluble collagen films as-cast and treated with EDC-NHS were characterised using PFM and QNM as controls to evaluate the piezoelectric effect of monomeric collagen aggregates.

Soluble collagen films seen in Fig. 7a revealed a network of worm-like structures approximately 100 nm wide. The lateral inphase data revealed that the individual fragments of soluble collagen possess a weak shear piezoelectric response, but no formation of larger micron-scale piezoelectric domains. Upon crosslinking with EDC-NHS, the fine collagen fragments were noted to produce thicker bundles roughly 200–300 nm. These bundles also produced a flattening of the lateral inphase as seen with the insoluble collagen sample, whilst enhancing the vertical inphase and amplitude response.

3 Discussion

3.1 Local mechanical effects of crosslinking

Although the effect of crosslinking on the bulk mechanical properties of collagen has been well studied, there has been limited characterisation at the local, cellular level. Global values are often obtained using compression testing for scaffolds[31] and tensile testing for films.[23] Mechanical properties measured using QNM exhibited a two-fold increase in elastic modulus upon crosslinking with EDC-NHS, and genipin at the highest concentrations. TG2-treated films also

experienced a two-fold increase in modulus at the lowest concentrations. No statistically significant differences were observed between the non-crosslinked samples and samples treated at the highest concentration of TG2. All modulus measurements of the collagen films were within the GPa scale. Measurements of the Young's modulus measured in the dry state of collagen are consistent with this scale. However, collagen-based tissues retain a significant level of water in their native states. Water content influences the chemical (and mechanical) behaviour of collagen through processes including protein hydration and protein induced structuring of water.[32] Mechanically, this effect is observed in the reduction in the Young's modulus by roughly an order of magnitude when moving from dry to hydrated samples.[33]

For comparison, films crosslinked with EDC-NHS and genipin have been shown to increase in their tensile modulus by one to two orders of magnitude under a hydrated tensile test[23,31,34] and exhibit Young's moduli at the MPa scale. Treatment with TG2 on the other hand resulted in films with moduli reduced by as much as an order of magnitude.[34] These results support previous findings where local mechanics of collagen vary significantly from the global properties, particularly when hydrated.[33]

Additionally, finite element modelling of nylon fibres that have been characterised using QNM has also shown significant differences in the measured modulus and piezoelectric response between nanowires and films of the same material.[18] The heterogeneity of the collagen fibre network may also result in the observed differences in values: in heterogeneously crosslinked pNIPAm hydrogels the average macroscopic Young's modulus was roughly 3 times the measured value by AFM.[35]

Furthermore, substrate stiffness has been reported to have a significant effect on the force curves obtained from AFM measurements when the deformation achieved is greater than 10% of the sample thickness.[36] The non-negligible effect of the substrate stiffness may hold not only for an AFM tip, but for cells that effectively act as probes for the surface properties. Since the collagen films produced are noted to have a large variation in thickness across the macroscopic sample (ESI, Fig. 21†), QNM and PFM are only used semi-quantitatively to identify the trends in this paper.

3.2 Structure and self-assembly of collagen fibres

The structure adopted by non-crosslinked collagen was observed to be dependent on the source of collagen used. For instance, insoluble collagen exhibited a rough surface as seen in Fig. 2i, whereas worm-like fragments were observed with soluble collagen in Fig. 7a. The topography of soluble collagen can be attributed the worm- or chain-like model that is often applied to flexible, single collagen protein molecules.[37] These flexible single collagen molecules can self-assemble into larger and more rigid rope-like fibrils through the process of fibrillogenesis.[38] Since the insoluble collagen used in this experiment was microfibrillar in nature, the worm-like fragments seen in soluble collagen were not observed on the insoluble collagen films.

EDC-NHS appears to result in self-assembly of the fibrils, or a pseudo-fibrillogenesis, particularly at the 100% crosslinking condition seen in Fig. 2. This self-assembly is dissimilar to the biologically observed fibrillogenesis, where self-assembly often results in the characteristic 67 nm banding on the fibrils formed.[39] In contrast, EDC-NHS crosslinking of extruded collagen fibres were observed to result in the loss of this characteristic binding.[40] This was suggested to arise through the disruption of the regular hydrogen bonding in biologically formed fibrils. The results of this paper emphasise the role played by carbodiimides in the self assembly of aligned fibre bundles without the need for an external method for fibre alignment such as extrusion.

3.3 Piezoelectric domains in collagen

The PFM images reveal that collagen films made from heavily processed and blended dermal collagen do not produce any perceptible piezoelectric domains that are consistent with the sample topography, whereas crosslinking with EDC-NHS allows fibre bundles to form with a localised piezoelectric response. Genipin and TG2 do not produce a localisation of the piezoelectric response unlike EDC-NHS. One interpretation of the increase in the vertical amplitude at the cost of the lateral could arise from the effect of domain orientation. The full piezoelectric tensor determined by Denning *et al.* revealed that individual collagen fibrils possess significant longitudinal piezoelectricity in addition to its shear components, leading to an underestimated global response across a sample with oppositely oriented domains.[7] Due to the effect of orientation, shear and lateral deformations may also be manifested as vertical ones due to buckling.[41] The loss of the shear piezoelectricity and gain of vertical piezoelectricity with EDC-NHS treatment may therefore arise from the anisotropy introduced in the collagen sample through fibre bundling. Moreover, although the net charge does not vary upon crosslinking with EDC-NHS, it must also be noted that the electron density available on an amine in the form a lone pair will undergo delocalisation in the π-system when crosslinked to form an amide. The reduced polarisability of the amide bond could therefore also result in the observed decrease in shear piezoelectricity.[42]

PFM images of soluble collagen films reveal worm-like structures which possess topographical correlation with the lateral amplitude and inphase of the piezoelectric response, unlike its insoluble collagen counterpart. This indicates that although the origin of piezoelectricity may be attributed to the ordering and charge imbalance of tropocollagen molecules, the large piezoelectric domains as observed in tendon[11] may be promoted by the crosslinking of the fibrils into large ordered structures. This is confirmed by previous reports on the piezoelectricity of evaporated and electrodeposited monomeric collagen films, which reveal that although evaporated films do not exhibit any strong fibrillar elements, they exhibit a small piezoelectric response when imaged using transmission electron microscopy.[4] Atomistic models in literature[8] also support the hypothesis that piezoelectric domains in col-

lagen are no larger than 50 Å, and likely to arise from the charge imbalance inherent in the tropocollagen molecule.

Additionally, the piezoelectric responses observed in this work only represent the trends under dry conditions. In a detailed study by Fukada *et al.* the piezoelectric constants of collagen were observed to have a large dependence on the hydration levels of the films produced.[24] In this study, increasing the hydration up to a maximum of 25% resulted in an increase the higher piezoelectric constants, around the freezing point of water. Above 25%, further hydration resulted in a drop in the piezoelectric properties at low temperatures. These phenomena were suggested to arise due to the role played by hydration in improving the ionic conductivity in either the piezoelectric or non-piezoelectric phases. Consequently, there is scope for further investigation regarding the role of hydration on the trends observed in this paper.

3.4 Local and global modifications to collagen piezoelectricity

In this study, we observe that EDC-NHS is able to produce a localised piezoelectric response, whereas genipin and tissue transglutaminase may alter the global values of piezoelectricity in a collagen sample. EDC-NHS is a zero length crosslinker, it is thought to be primarily a intra-fibrillar crosslinker due to the requirement for nearest neighbour amidation. However, in light of the fibre bundle self-assembly observed, we suggest that EDC-NHS can also produce inter-fibrillar crosslinking, producing bundles of roughly 300 nm at the highest concentrations, as seen in the width of the collagen fibre bundles formed in both the insoluble and soluble collagen films post-crosslinking (Fig. 6a and 7a). As illustrated schematically in Fig. 8, fibres crosslinked *via* intra-fibrillar crosslinking could locally align the fibrils, resulting in a localisation of the piezoelectric response along the fibres.

Non-localised piezoelectric enhancement of the piezoelectric response was observed with TG2 and genipin treatments of insoluble collagen. Charge carrying amino acids on the collagen backbone can exists in both their protonated and deprotonated states. The interaction of genipin and TG2 with these charge carrying entities may be responsible for this observed increase in piezoelectricity. TG2 can facilitate the conversion of charge-neutral glutamines at high concentrations,[29] allowing negatively charged glutamates to be produced in place of amide bonds (Fig. 8). On the other hand, the genipin molecule reacts with primary amines to form crosslinks with collagen,[28] resulting a reduction of positively charged side groups.

Moreover, this interpretation is consistent with the characterisation of surface charge using a single glycated collagen fibril by Mesquida *et al.* The presence of negative carbonyl containing compounds upon crosslinking with glutaraldehyde was observed to reduce the surface potential.[43] This is similar to the decrease in surface potential and introduction of gluta-

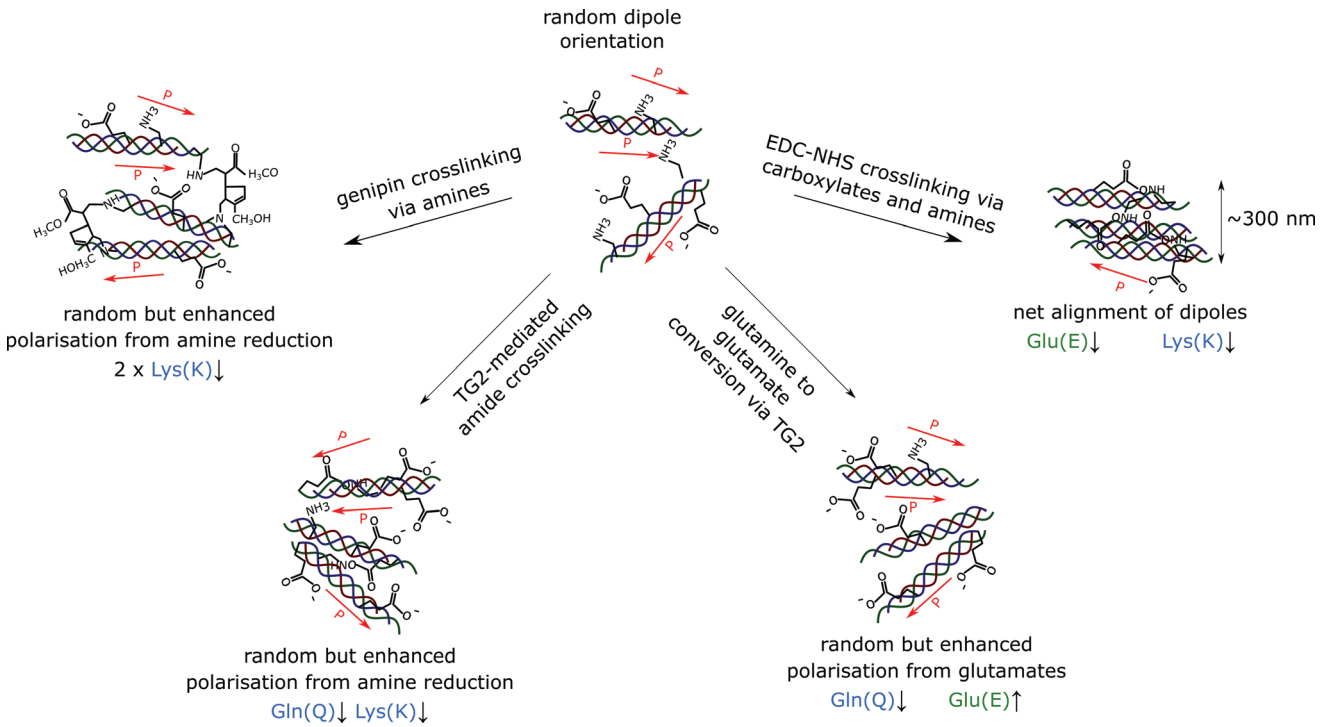

Fig. 8 Suggested modes of amino-acid level modification of piezoelectricity *via* crosslinking. Inter-fibril EDC-NHS crosslinking produces fibres of roughly 300 nm exhibiting a piezoelectric response from fibril alignment, despite a reduction in charge carriers on the collagen backbone. TG2 can produce additional negatively charged glutamates on the collagen backbone or remove a glutamine and lysine to form an amide crosslink, whereas genipin consumes the positively charged amines during crosslinking. All three mechanisms result in the enhancement of the net polarisation. Labels in green represent negatively charged amino acids, whereas labels in blue represent positively charged amino acids.

Table 1 Table listing the nomenclature given to crosslinkers used in this study, their standard reaction concentrations as well as their degrees of crosslinking as determined from a ninhydrin free amine assay by Nair *et al.*[34]

Crosslinker	Concentration	Degree of crosslinking
EDC-NHS (low)	10%	17%
EDC-NHS (medium)	50%	47%
EDC-NHS (high)	100%	52%
Genipin (low)	60%	16%
Genipin (medium)	100%	28%
Genipin (high)	200%	35%
TG2 (low)	40%	50%
TG2 (medium)	100%	48%
TG2 (high)	200%	46%

mates (carboxylates) through crosslinking *via* TG2 described in Fig. 5 and 8.

The loss of the charged amino acid side groups upon crosslinking may be responsible for the loss of the shear piezoelectric response in collagen, whilst enhancing the vertical piezoelectric response. Chemical crosslinking of collagen therefore represents one of the first experimental examples of amino-acid level modification of piezoelectricity in collagen. Such behaviour has previously been hypothesised by other studies considering the inherent piezoelectricity of the building blocks of collagen.[6]

4 Conclusions

Carbodiimide crosslinking of collagen films results in local alignment of collagen fibrils to form thicker fibre bundles of 300 nm, with a perceptible enhanced and localised vertical piezoelectric response. TG2 and genipin crosslinked films on the other hand display a non-localised yet enhanced piezoelectric response upon crosslinking. The localisation of piezoelectricity in EDC-NHS crosslinked collagen films, as well as the enhancement of piezoelectricity in TG2- and genipin-treated films are proposed to arise from changes to the charge carrying amino-acid groups. This gives the potential to exploit the structure of collagen using crosslinking and other chemical modifications in order to tailor of electromechanical properties. As a result, we can begin to consider not only the biological response to such phenomena, but also to expand the range of design considerations and modifiable parameters currently used with collagen-based tissue engineering implants to include local mechanical and piezoelectric properties.

5 Materials and methods

5.1 Collagen film fabrication

5.1.1 Microfibrillar insoluble collagen. A 0.5% suspension of Type I dermal microfibrillar bovine collagen (Devro Medical, Moodiesburn, Scotland) was prepared in 0.05 M acetic acid solution (Alfa Aesar) and left to swell overnight at 4 °C. Suspensions were homogenised at 22 000 rpm for four minutes in total using a commercial blender (Waring model 8011EG). The resulting suspension was degassed under vacuum to remove any air bubbles. Films were prepared by drop-casting 400 μl of the suspension to an ITO coated glass cover slip (Sigma Aldrich). Films were left to dry for 48 hours before crosslinking.

5.1.2 Soluble collagen. Films were prepared by adding 400 μl of a 0.31% solution of Type I dermal acid-soluble bovine collagen in 0.05 M acetic acid solution to an ITO coated glass cover slip (Sigma Aldrich). Films were left to dry for 48 hours before crosslinking.

5.2 Crosslinking

5.2.1 EDC-NHS. A crosslinking solution of 1-ethyl-3-(3-dimethylaminopropyl) carbodiimide hydrochloride (EDC, Sigma-Aldrich) and *N*-hydroxysuccinimide (NHS, Sigma-Aldrich) was prepared using a 5 : 2 : 1 molar ratio for EDC : NHS : collagen, hereby referred to as the '100% concentration'. For every 1 g of collagen the 100% concentration standard of crosslinking solution consisted of 1.15 g EDC and 0.276 g NHS dissolved in 75% ethanol. Diluted crosslinking solutions were prepared at a molar ratio of 5 : 2 : 2 and 5 : 2 : 10 EDC : NHS : collagen, hereby referred to as the '50%' and '10%' crosslinking concentrations for EDC-NHS. Films were immersed in 100% ('high'), 50% ('medium') and 10% ('low') crosslinking solution for 2 hours at ambient temperature.

5.2.2 Genipin. Using a mass for mass equivalence for genipin to PBS adapted from the protocol by Zhang *et al.*,[44] for every 1 g of collagen the 100% concentration standard of crosslinking solution consisted of 0.7812 g of genipin (Challenge Bioproducts 160919) dissolved in PBS (Sigma Aldrich). Crosslinking solutions prepared at a mass ratio of 1.5624 g of genipin per gram of collagen are referred to as the '60%' and mass ratio of 0.46872 g genipin per gram of collagen referred to as the '200%' crosslinking concentrations for genipin. Samples were immersed in 60% ('low'), 100% ('medium') and 200% ('high') crosslinking solution for 24 hours at ambient temperature.

5.2.3 Tissue transglutaminase 2. Using a mass for mass equivalence for TG2 and Tris in the protocol adopted by Chau *et al.*,[45] for every 1 g of collagen the 100% concentration standard of crosslinking solution consisted of 1 mg of TG2 (Sigma Aldrich) dissolved in Tris Buffer pH 7.5 (Sigma Aldrich) and 5 mM $CaCl_2$ (Sigma Aldrich). Solutions prepared with 0.4 mg of TG2 per gram of collagen and 2.0 mg of TG2 per gram of collagen are referred to as the '40%' and '200%' crosslinking concentrations for TG2. Samples were immersed in 40% ('low'), 100% ('medium') and 200% ('high') crosslinking solutions for 24 hours at 37 °C.

All crosslinked films were washed rapidly with distilled water (10 seconds × 4) followed by soaking in distilled water for longer intervals (15 minutes × 4). Films were left to dry for 48 hours before use. Degrees of crosslinking as determined by a ninhydrin free amine assay by Nair *et al.* are listed in Table 1.[34]

5.3 Atomic force microscopy

All samples were fixed with silver paint onto stainless steel specimen discs (Agar Scientific) and imaged using the MultiMode 8 (Bruker) atomic force microscope.

5.3.1 Quantitative nanomechanical mapping. Quantitative Nanomechanical Mapping (QNM) in peak force mode was used to image 5 × 5 μm areas recording surface topography, deformation, dissipation, adhesion and DMT Modulus of each film in dry conditions. For each set of measurements (n = 3), a single Tap300Al-G tip (Budget Sensors) was used for which deflection sensitivity was calibrated on a sapphire substrate and AFM parameters set to fit a PS-LDPE standard. NanoScope ScanAsyst was used to optimise gain, scan rate and set point. A second set of films was produced on borosilicate microscope cover slips (Scientific Laboratory Supplies) to verify observed trends and check for substrate effects (n = 3). Complete information from all QNM channels are presented in ESI, Fig. 1–9.†

5.4 Piezoresponse force microscopy

Samples from six selected conditions (insoluble collagen, soluble collagen, 100% EDC-NHS-, 100% genipin- and 100% TG2-treated insoluble collagen, and 100% EDC-NHS cross-linked soluble collagen) were chosen for piezoresponse force microscopy imaging. Kelvin Force Probe Microscopy (KPFM) in tapping mode was used to image 2.5 × 5 μm areas recording surface topography and potential in dry conditions, (n = 3). (Channels shown in ESI, Fig. 10–12†) piezoresponse force microscopy was subsequently used in contact mode to image the same 5 μm × 5 μm area with a AC lock-in amplitude of 4000 mV, and DC offset set to the surface potential measured during KPFM. The surface topography, in-phase and out-of-phase amplitudes and quadratures were recorded as channels during this measurement in dry conditions. For each set of measurements, a single conductive MESP-RC-V2 tip (tip width = 35 nm, spring constant = 5.1925 N m^{-1}) was used. NanoScope ScanAsyst was also enabled to optimise gain, scan rate and set point. The height, vertical and lateral inphase and lateral amplitude channels are shown here, with representative images of all other channels in ESI, Fig. 13–19.†

5.5 Image processing and data analysis

Analysis of images from all channels were then performed using *Gwyddion* and the batch processing module Pygwy.

5.5.1 Image processing. All images were processed using the align rows and horizontal scar removal tools to remove the effect of scanner drift. The data minimum was fixed to zero to allow semi-quantitative comparison of the distribution across the imaged area. The data were then flattened using a polynomial background removal.

5.5.2 Quantitative analysis. Basic statistical quantities including the mean and median values were computed using in-built functions in *Gwyddion* for each area prior to any image processing. The median values for each area were then averaged and quoted as the arithmetic mean ± standard deviation for each condition (n = 3).

5.5.3 Statistical analysis. Since Levene's test for homoscedasticity and Anderson–Darling normality were not passed by the datasets, the non-parametric Mann–Whitney test was used to identify groups with $p > \alpha$ when compared with the non-cross-linked standards. α = 0.05 except where otherwise stated.

Conflicts of interest

There are no conflicts to declare.

Acknowledgements

SKN and YC acknowledge financial support from the ERC Starting Grant 639526, NANOGEN. REC and SMB acknowledge the supported by the EPSRC Established Career Fellowship Grant No. EP/N019938/1. Open Access is funded by the Bill and Melinda Gates Foundation OPP1144. MN acknowledges the financial support provided by the Gates Cambridge Trust and Geistlich Pharma AG to undertake this research. Data is available on the University of Cambridge Apollo Open Data Repository at http://dx.doi.org/10.17863/CAM.40297.

References

1 M. H. Shamos and L. S. Lavine, Piezoelectricity as a fundamental property of biological tissues, *Nature*, 1967, **213**(5073), 267.
2 M. Xue and C. J. Jackson, Extracellular matrix reorganization during wound healing and its impact on abnormal scarring, *Adv. Wound Care*, 2015, **4**(3), 119–136.
3 K. R. Robinson, The responses of cells to electrical fields: a review, *J. Cell Biol.*, 1985, **101**(6), 2023–2027.
4 A. A. Marino, J. A. Spadaro, E. Fukada, L. D. Kahn and R. Becker, Piezoelectricity in collagen films, *Calcif. Tissue Int.*, 1980, **31**(1), 257–259.
5 E. Fukada and I. Yasuda, Piezoelectric effects in collagen, *Jpn. J. Appl. Phys.*, 1964, **3**(2), 117.
6 S. Guerin, T. A. Syed and D. Thompson, Deconstructing collagen piezoelectricity using alanine-hydroxyproline-glycine building blocks, *Nanoscale*, 2018, **10**(20), 9653–9663.
7 D. Denning, J. I. Kilpatrick, E. Fukada, N. Zhang, S. Habelitz, A. Fertala, M. D. Gilchrist, Y. Zhang, S. A. Tofail and B. J. Rodriguez, Piezoelectric tensor of collagen fibrils determined at the nanoscale, *ACS Biomater. Sci. Eng.*, 2017, **3**(6), 929–935.
8 Z. Zhou, D. Qian and M. Minary-Jolandan, Molecular mechanism of polarization and piezoelectric effect in super-twisted collagen, *ACS Biomater. Sci. Eng.*, 2016, **2**(6), 929–936.
9 M. Minary-Jolandan and M.-F. Yu, Nanoscale characterization of isolated individual type i collagen fibrils: polarization and piezoelectricity, *Nanotechnology*, 2009, **20**(8), 085706.

10 D. Denning, J. Kilpatrick, T. Hsu, S. Habelitz, A. Fertala and B. Rodriguez, Piezoelectricity in collagen type ii fibrils measured by scanning probe microscopy, *J. Appl. Phys.*, 2014, **116**(6), 066818.
11 C. P. Brown, J. L. Boyd, A. J. Palmer, M. Phillips, C.-A. Couture, M. Rivard, P. A. Hulley, A. J. Price, A. Ruediger, F. Légaré, *et al.*, Modulation of mechanical interactions by local piezoelectric effects, *Adv. Funct. Mater.*, 2016, **26**(42), 7662–7667.
12 C. P. Brown, C. Harnagea, H. S. Gill, A. J. Price, E. Traversa, S. Licoccia and F. Rosei, Rough fibrils provide a toughening mechanism in biological fibers, *ACS Nano*, 2012, **6**(3), 1961–1969.
13 T. Glatzel, H. Hölscher, T. Schimmel, M. Z. Baykara, U. D. Schwarz and R. Garcia, Advanced atomic force microscopy techniques, *Beilstein J. Nanotechnol.*, 2012, **3**, 893.
14 C. Su, J. Shi, Y. Hu, S. Hu and J. Ma, Method and apparatus of using peak force tapping mode to measure physical properties of a sample, *US Pat.*, 9995765, 2016.
15 Y. Calahorra, A. Datta, J. Famelton, D. Kam, O. Shoseyov and S. Kar-Narayan, Nanoscale electromechanical properties of template-assisted hierarchical self-assembled cellulose nanofibers, *Nanoscale*, 2018, **10**(35), 16812–16821.
16 Y. Calahorra, R. A. Whiter, Q. Jing, V. Narayan and S. Kar-Narayan, Localized electromechanical interactions in ferroelectric P(VDF-TRFE) nanowires investigated by scanning probe microscopy, *APL Mater.*, 2016, **4**(11), 116106.
17 R. A. Whiter, Y. Calahorra, C. Ou and S. Kar-Narayan, Observation of confinement-induced self-poling effects in ferroelectric polymer nanowires grown by template wetting, *Macromol. Mater. Eng.*, 2016, **301**(9), 1016–1025.
18 Y. S. Choi, S. K. Kim, F. Williams, Y. Calahorra, J. A. Elliott and S. Kar-Narayan, The effect of crystal structure on the electromechanical properties of piezoelectric nylon-11 nanowires, *Chem. Commun.*, 2018, 6863–6866.
19 M. Smith, Y. Calahorra, Q. Jing and S. Kar-Narayan, Direct observation of shear piezoelectricity in poly-l-lactic acid nanowires, *APL Mater.*, 2017, **5**(7), 074105.
20 E. Soergel, Piezoresponse force microscopy (PFM), *J. Phys. D: Appl. Phys.*, 2011, **44**(46), 464003.
21 S. Kim, D. Seol, X. Lu, M. Alexe and Y. Kim, Electrostatic-free piezoresponse force microscopy, *Sci. Rep.*, 2017, **7**, 41657.
22 N. Davidenko, C. F. Schuster, D. V. Bax, R. W. Farndale, S. Hamaia, S. M. Best and R. E. Cameron, Evaluation of cell binding to collagen and gelatin: a study of the effect of 2D and 3D architecture and surface chemistry, *J. Mater. Sci.: Mater. Med.*, 2016, **27**(10), 148.
23 C. N. Grover, J. H. Gwynne, N. Pugh, S. Hamaia, R. W. Farndale, S. M. Best and R. E. Cameron, Crosslinking and composition influence the surface properties, mechanical stiffness and cell reactivity of collagen-based films, *Acta Biomater.*, 2012, **8**(8), 3080–3090.
24 E. Fukada, H. Ueda and R. Rinaldi, Piezoelectric and related properties of hydrated collagen, *Biophys. J.*, 1976, **16**(8), 911–918.
25 A. Bazaid, S. M. Neumayer, A. Sorushanova, J. Guyonnet, D. Zeugolis and B. J. Rodriguez, Non-destructive determination of collagen fibril width in extruded collagen fibres by piezoresponse force microscopy, *Biomed. Phys. Eng. Express*, 2017, **3**(5), 055004.
26 L. Olde Damink, P. Dijkstra, M. Van Luyn, P. Van Wachem, P. Nieuwenhuis and J. Feijen, Cross-linking of dermal sheep collagen using a water-soluble carbodiimide, *Biomaterials*, 1996, **17**(8), 765–773.
27 J. W. Keillor, C. M. Clouthier, K. Y. Apperley, A. Akbar and A. Mulani, Acyl transfer mechanisms of tissue transglutaminase, *Bioorg. Chem.*, 2014, **57**, 186–197.
28 N. Tambe, J. Di, Z. Zhang, S. Bernacki, A. El-Shafei and M. W. King, Novel genipin-collagen immobilization of polylactic acid (PLA) fibers for use as tissue engineering scaffolds, *J. Biomed. Mater. Res., Part B*, 2015, **103**(6), 1188–1197.
29 J. Stamnaes, B. Fleckenstein and L. M. Sollid, The propensity for deamidation and transamidation of peptides by transglutaminase 2 is dependent on substrate affinity and reaction conditions, *Biochim. Biophys. Acta, Proteins Proteomics*, 2008, **1784**(11), 1804–1811.
30 Y. Calahorra, M. Smith, A. Datta, H. Benisty and S. Kar-Narayan, Mapping piezoelectric response in nanomaterials using a dedicated non-destructive scanning probe technique, *Nanoscale*, 2017, **9**(48), 19290–19297.
31 M. G. Haugh, C. M. Murphy, R. C. McKiernan, C. Altenbuchner and F. J. O'Brien, Crosslinking and mechanical properties significantly influence cell attachment, proliferation, and migration within collagen glycosaminoglycan scaffolds, *Tissue Eng., Part A*, 2011, **17**(9–10), 1201–1208.
32 G. D. Fullerton and M. R. Amurao, Evidence that collagen and tendon have monolayer water coverage in the native state, *Cell Biol. Int.*, 2006, **30**(1), 56–65.
33 L. Yang, K. O. Van der Werf, C. F. Fitié, M. L. Bennink, P. J. Dijkstra and J. Feijen, Mechanical properties of native and cross-linked type I collagen fibrils, *Biophys. J.*, 2008, **94**(6), 2204–2211.
34 M. Nair, R. K. Johal, S. M. Best and R. E. Cameron, Tunable bioactivity and mechanics of collagen-based tissue engineering constructs: A comparison of EDC-NHS, genipin and TG2 crosslinkers, 2019, DOI: 10.17863/CAM.36098.
35 F. Di Lorenzo, J. Hellwig, R. von Klitzing and S. Seiffert, Macroscopic and microscopic elasticity of heterogeneous polymer gels, *ACS Macro Lett.*, 2015, **4**(7), 698–703.
36 G. Thomas, N. A. Burnham, T. A. Camesano and Q. Wen, Measuring the mechanical properties of living cells using atomic force microscopy, *J. Visualized Exp.*, 2013, (76), 50497.
37 S.-W. Chang and M. J. Buehler, Molecular biomechanics of collagen molecules, *Mater. Today*, 2014, **17**(2), 70–76.

38 K. E. Kadler, Fell Muir lecture: Collagen fibril formation in vitro and in vivo, *Int. J. Exp. Pathol.*, 2017, **98**(1), 4–16.
39 J. R. Harris, A. Soliakov and R. J. Lewis, In vitro fibrillogenesis of collagen type I in varying ionic and pH conditions, *Micron*, 2013, **49**, 60–68.
40 D. Shepherd, J. Shepherd, S. Ghose, S. Kew, R. Cameron and S. Best, The process of EDC-NHS cross-linking of reconstituted collagen fibres increases collagen fibrillar order and alignment, *APL Mater.*, 2015, **3**(1), 014902.
41 S. V. Kalinin, B. J. Rodriguez, S. Jesse, J. Shin, A. P. Baddorf, P. Gupta, H. Jain, D. B. Williams and A. Gruverman, Vector piezoresponse force microscopy, *Microsc. Microanal.*, 2006, **12**(3), 206–220.
42 A. A. Gagrai, V. R. Mundlapati, D. K. Sahoo, H. Satapathy and H. S. Biswal, The role of molecular polarizability in designing organic piezoelectric materials, *ChemistrySelect*, 2016, **1**(14), 4326–4331.
43 P. Mesquida, D. Kohl, O. G. Andriotis, P. J. Thurner, M. Duer, S. Bansode and G. Schitter, Evaluation of surface charge shift of collagen fibrils exposed to glutaraldehyde, *Sci. Rep.*, 2018, **8**, 10126.
44 X. Zhang, X. Chen, T. Yang, N. Zhang, L. Dong, S. Ma, X. Liu, M. Zhou and B. Li, The effects of different crossing-linking conditions of genipin on type I collagen scaffolds: an in vitro evaluation, *Cell Tissue Banking*, 2014, **15**(4), 531–541.
45 D. Y. Chau, R. J. Collighan, E. A. Verderio, V. L. Addy and M. Griffin, The cellular response to transglutaminase-cross-linked collagen, *Biomaterials*, 2005, **26**(33), 6518–6529.